Supplementary Information

Dominant role of OH^- and Ti interstitial defects on the electronic structure of TiO_2 thin films for water splitting

Maria-Isabel Mendoza-Diaz,[a] Andrea Balocchi,[b] Kolade A. Oyekan,[c] Kui Tan,[c] William G. Vandenberghe, [c] Alain Esteve[a] and Carole Rossi*[a]

[a] *LAAS-CNRS, University of Toulouse, 7 Avenue du colonel Roche, 31400 Toulouse, France*

[b] *INSA-CNRS-UPS, LPCNO, University of Toulouse, 135 avenue de Rangueil, 31077 Toulouse, France*

[c] *Department of Materials Science and Engineering, University of Texas at Dallas, Richardson, TX (USA)*

* Corresponding Author.

E-mail: rossi@laas.fr, (C. Rossi). Tel. +33-05-6133-6301

Keywords: TiO_2, photocatalyst, photoluminescence, H_2 production, water splitting, band structure

S1. Structural, morphological and mechanical properties

Crystallite diameter calculation with Scherrer's formula

The respective crystallite diameter for the anatase and rutile was be estimated from the GI-XRD pattern using the Scherrer's formula [1]:

$$D_{hkl} = \frac{k\,\lambda}{\beta_{hkl}\,cos\theta} \qquad \text{(Eq. S2)}$$

Where k is the shape factor for Cu target (0.89), λ is the X-ray wavelength of the Cu Kα radiation (0.154 nm), θ is the Bragg's angle of anatase (101) and rutile (110) peaks, and β is the full-width half-maximum (FWHM) of the corresponding diffraction peak.

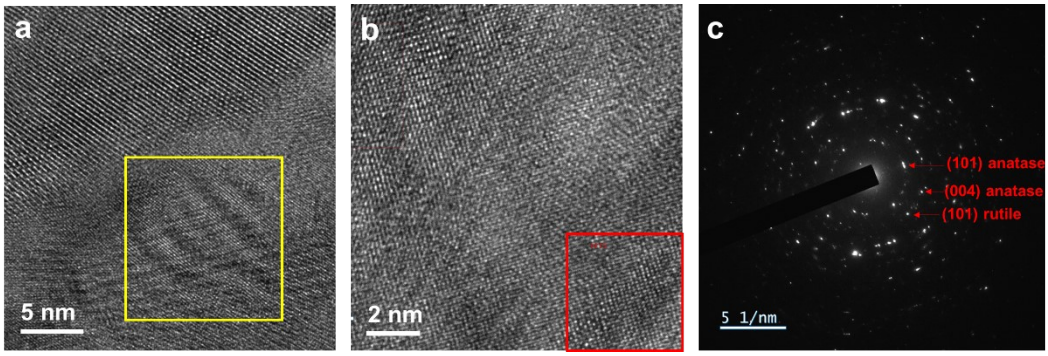

Figure S1-1 *High-resolution images of TiO_2 film as deposited on silicon (T-AD) (a) square showing the Moiré fringes resulted from the combination of lattice fringes of anatase and rutile, (b) cross-section depicting the selected area for the selected area electron diffraction (SAED). (c) Electron diffraction pattern, anatase and rutile planes determined from the inverse of the radius ring.*

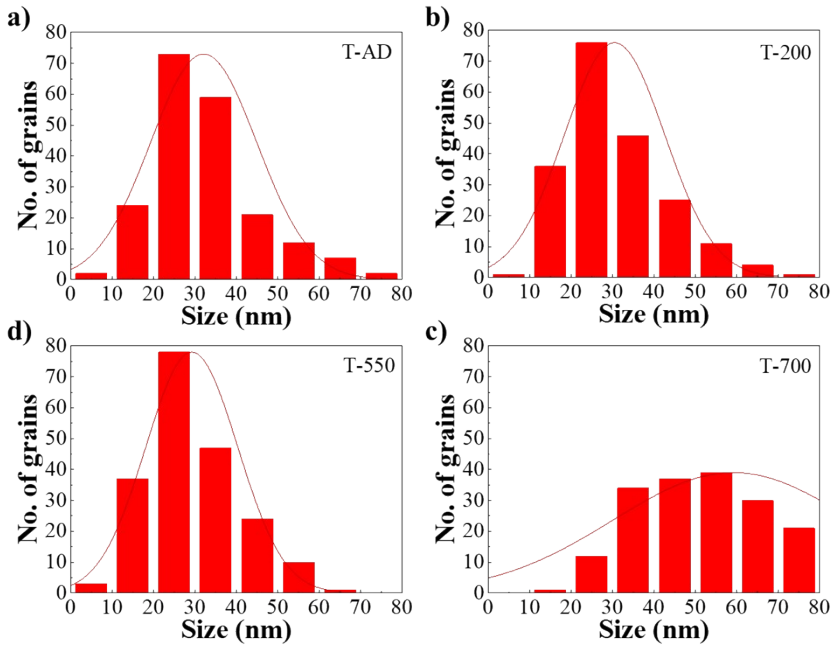

Figure S1-2. *Grain size distribution obtained from SEM measurements for TiO2 films on silicon (a) as-deposited, and annealed at (b) 200, (c) 550 and (d) 700°C.*

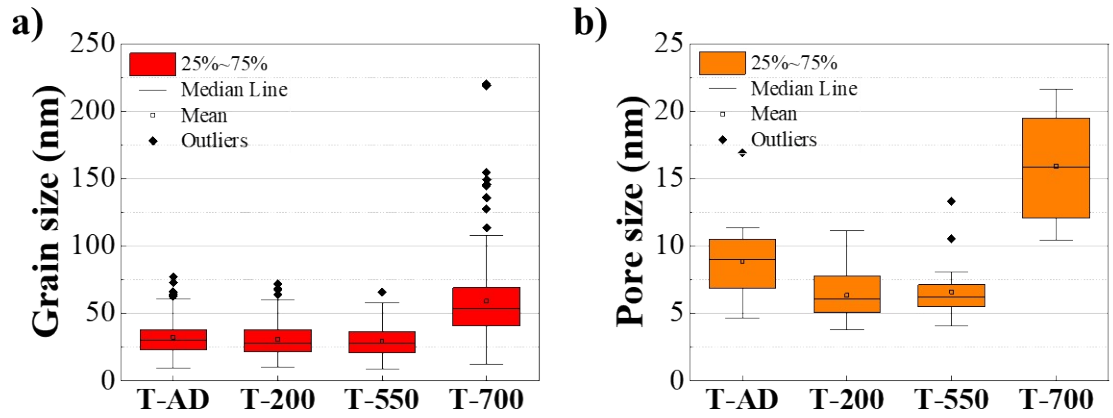

Figure S1-3. *(a) Grain and (b) pore size distribution obtained from SEM measurements for TiO2 films on silicon (a) as-deposited, and annealed at (b) 200, (c) 550 and (d) 700°C.*

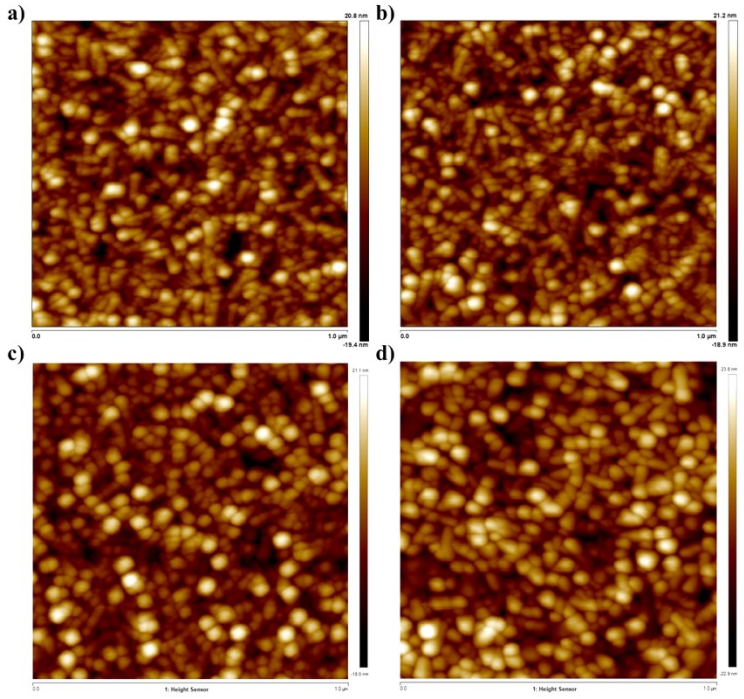

Figure S1-4. *2D AFM* images *of TiO_2 films deposited on silicon (a) as-deposited, and annealed at (b) 200, (c) 550 and (d) 700°C.*

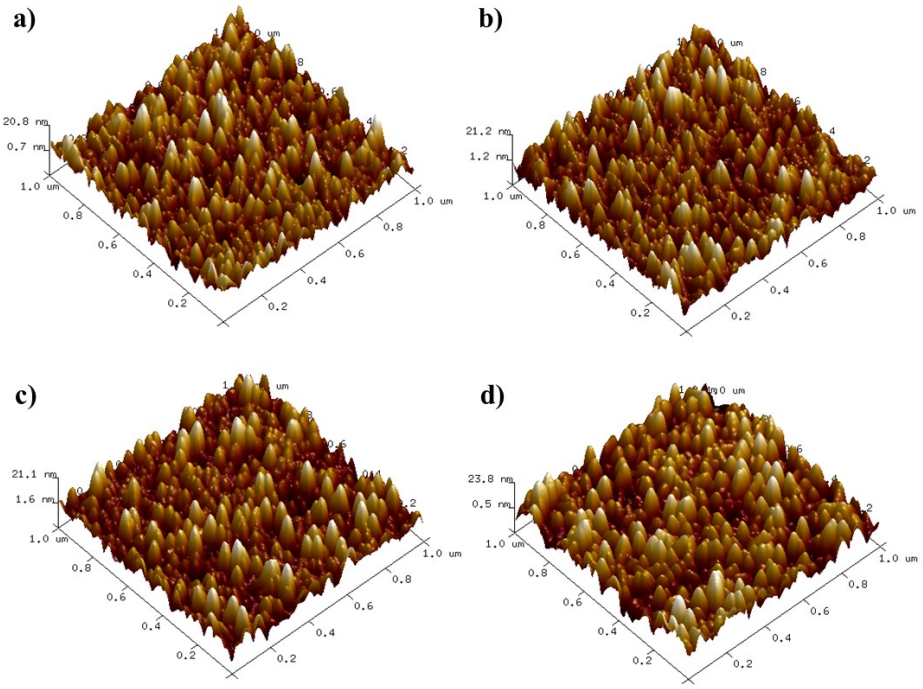

Figure S1-5 *3D AFM* images *of TiO_2 films deposited on silicon (a) as-deposited, and annealed at (b) 200, (c) 550 and (d) 700°C.*

Tensile stress test calculation

The residual stress was estimated by measuring the radii of curvature of bare silicon substrates and the substrates with the as-deposited and annealed films. After measuring the radii of curvature R due to bending, the residual stress (σ) is calculated by using Stoney's equation [2]:

$$\sigma = \frac{E_s \quad t_s^2}{6(1-v_s)t_c}\left(\frac{1}{R}-\frac{1}{R_0}\right) \qquad \text{(Eq. S2)}$$

Where E_s, v_s, t_s and t_c are the Young's modulus, Poisson ratio and thickness of the substrate (500 um) and film (0.27 um). R_0 and R are radii of curvature of the bare substrate and sample film-substrate, respectively.

Table S1. *Average residual tensile stress parameters of TiO_2 thin films.*

Sample	Average Stress (MPa)	R (m)	Std. Dev. (MPa)
T-AD	191.00	160.8	$7.46\ 10^{-8}$
T-200	315.50	97.35	$7.78\ 10^{-8}$
T-550	605.50	50.72	$8.24\ 10^{-8}$
T-700	638.30	48.11	$7.76\ 10^{-8}$

S2. H_2 evolution

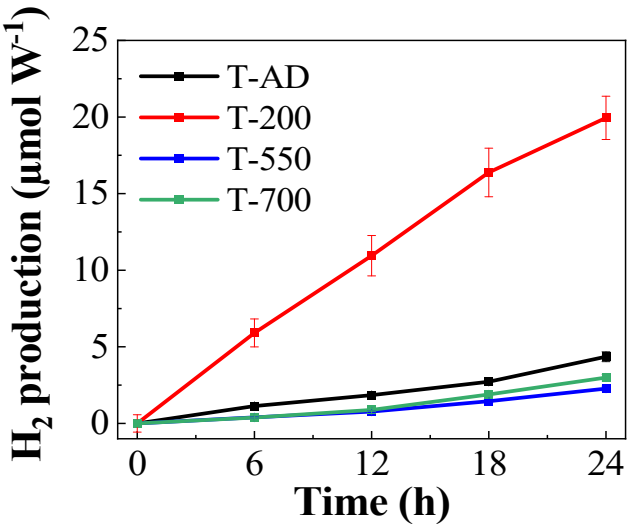

Figure S2. *Hydrogen production over 24 h of TiO_2 films deposited on silicon: as-deposited (T-AD) and annealed at 200 (T-200), 550 (T-550) and 700°C (T-700). Xe lamp used for irradiation.*

S3. Chemical characterization

Table S3. *Details of XPS spectra binding energies of TiO_2 thin films. BE in eV.*

Samples	Ti^{4+} ($2p_{3/2}$)	Ti^{3+} ($2p_{3/2}$)	Ti^{4+} ($2p_{1/2}$)	Ti^{3+} ($2p_{1/2}$)	O1s HE	O1s LE
T-AD	459.16	457.72	464.86	463.32	532.82	530.37
T-200	458.85	457.51	464.53	463.11	532.46	530.06
T-550	458.94	457.46	464.63	463.06	531.39	530.12
T-700	458.71	457.23	464.41	462.93	531.88	530.36

Calculation of TiO_2 surface stoichiometry

The stoichiometry of the TiO_2 surface, in terms of O^{2-}/Ti^{4+} atomic ratio was calculated from the mathematical area I of the O 1s Low Energy component (O-Ti) and the Ti $2p_{2/3}$ and $2p_{1/2}$ peaks, of the XPS O1s and Ti2p core level spectra as follows:

$$\frac{O}{Ti} = \frac{I_O}{I_{Ti\,2p_{\frac{1}{2}}} + I_{Ti\,2p_{\frac{3}{2}}}} \qquad \text{(Eq. S4)}$$

S4. Optical properties

The absorption coefficient α, was determined from the transmittance spectra, using the expression [3]:

$$\alpha = \frac{\ln\left(\frac{1}{T}\right)}{d} \qquad \text{(Eq. S5-1)}$$

Where T is the transmittance of the film at teach wavelength and d is the thickness of the film in cm.

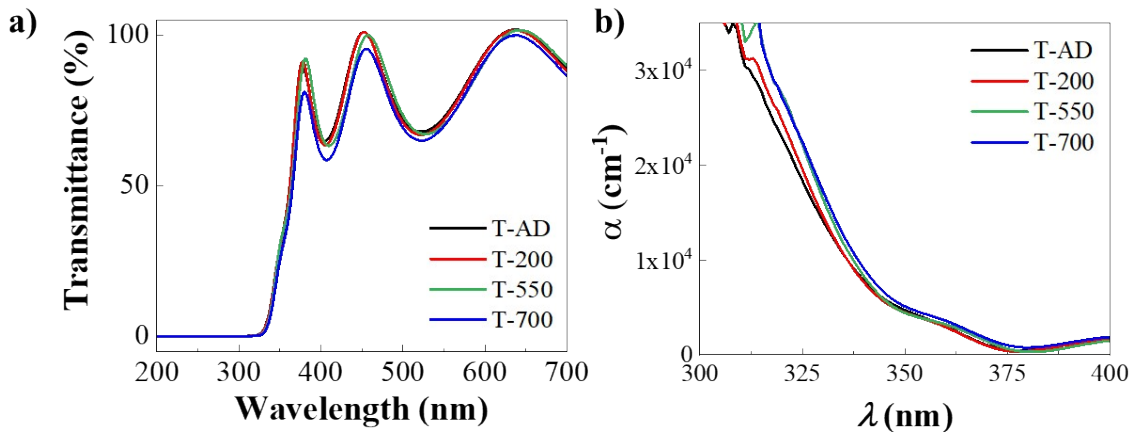

Figure S4-1. *(a) UV-vis transmittance spectra and (b)Absorption coefficient spectra of TiO_2 films deposited on quartz (determined from transmittance spectra).*

The absorption edge was estimated from the absorption coefficient in the exponential tail with values of $\alpha < 1\ 10^4$ cm^{-1} with a linear fitting where $R^2 = 0.99$ [4]. The absorption edge values are reported in **Table S4.**

Table S4. *Absorption edge of TiO_2 thin films determined from transmittance spectra.*

Samples	Absorption edge (nm)
T-AD	356.13
T-200	354.02
T-550	354.07

T-700	357.29

The optical band gap E_g was calculated from using the relation [4]:

$$\alpha hv \propto (hv - E_g)^n \qquad \text{(Eq. S5-2)}$$

Where hv is the photon energy (eV) and n is 2 for the indirect allowed transition in TiO_2. The Tauc plots were obtained by plotting $(\alpha hv)^{\frac{1}{2}}$ versus hv as shown in the **Figure S7a**. The slope located at high energies was extrapolated by linear fit to the baseline ($R^2 = 0.99$).

The Urbach energy E_u is defined by [5]:

$$\alpha = \alpha_0 \left(\frac{hv}{E_u}\right) \qquad \text{(Eq. S5-3)}$$

Where is α is the previously mentioned absorption coefficient and α_0 is a constant. The Urbach energy is calculated by plotting $\ln \alpha$ versus hv as shown in the **Figure S5-2b**. The reciprocal of the slope in the linear portion gives the E_u.

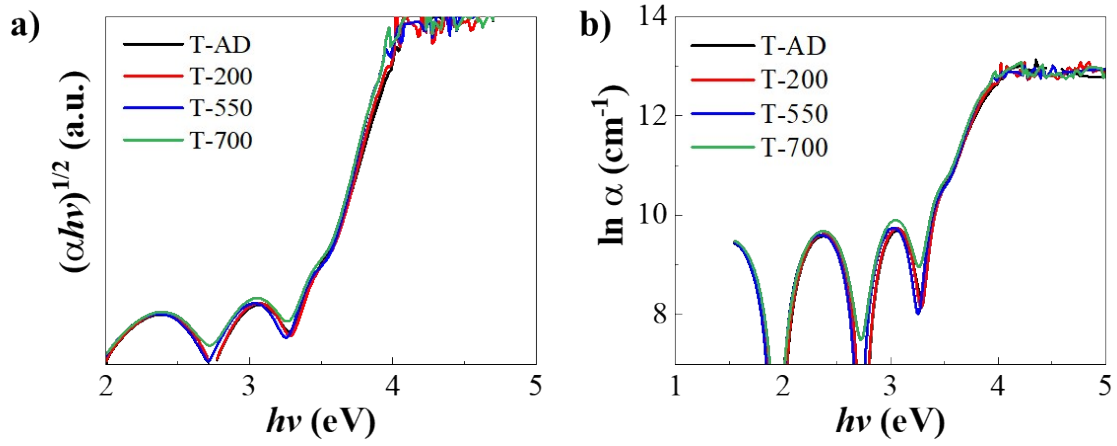

Figure S4-2. *(a) Tauc plots and (b) Plot of* $\ln \alpha$ *versus* hv *for the Ubarch energy determination of* TiO_2 *films deposited by PVD on quartz. Plots determined from transmittance spectra.*

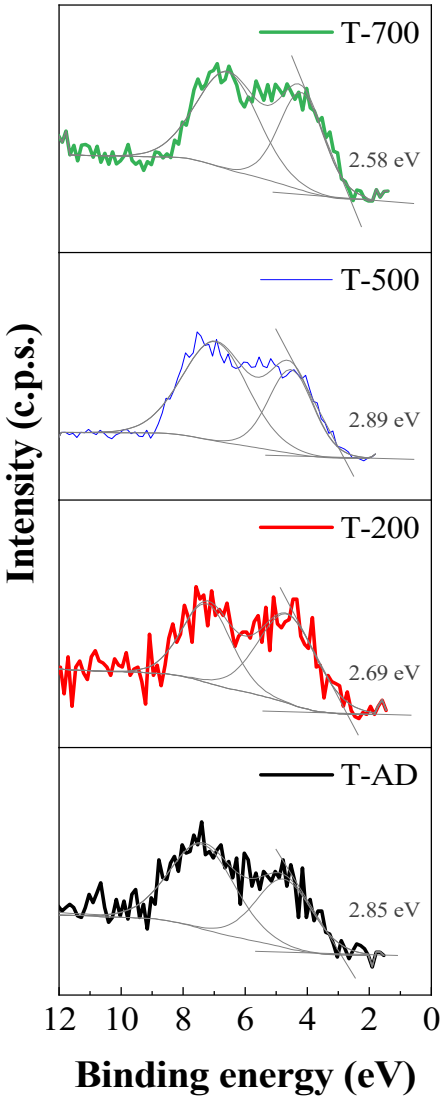

Figure S4-3. *Calculated valence band edge of TiO_2 films as-deposited (T-AD) and annealed at 200 (T-200), 550 (T-500) and 700 °C (T-700). Lines indicate the intersection of the TiO_2 O2p orbital with the baseline.*

S5. PL measurements

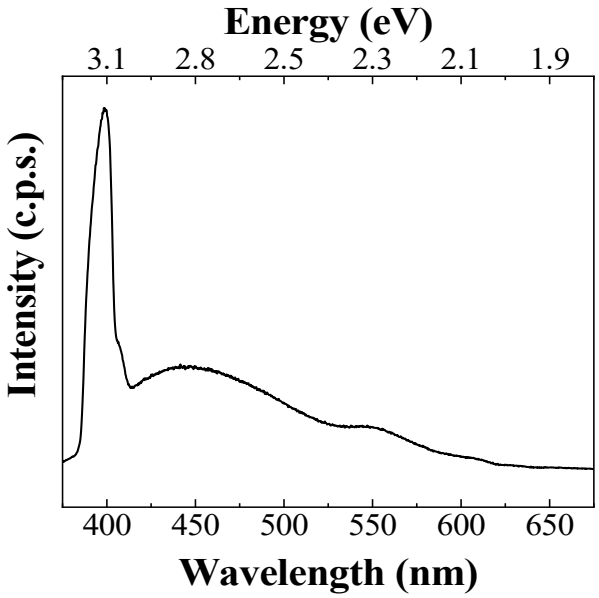

Figure S5. *Photoluminescence spectra at room temperature of ethanol excited at 355 nm.*

Ethanol in quartz cell.

S6. Density functional theory (DFT) calculations

Computational details

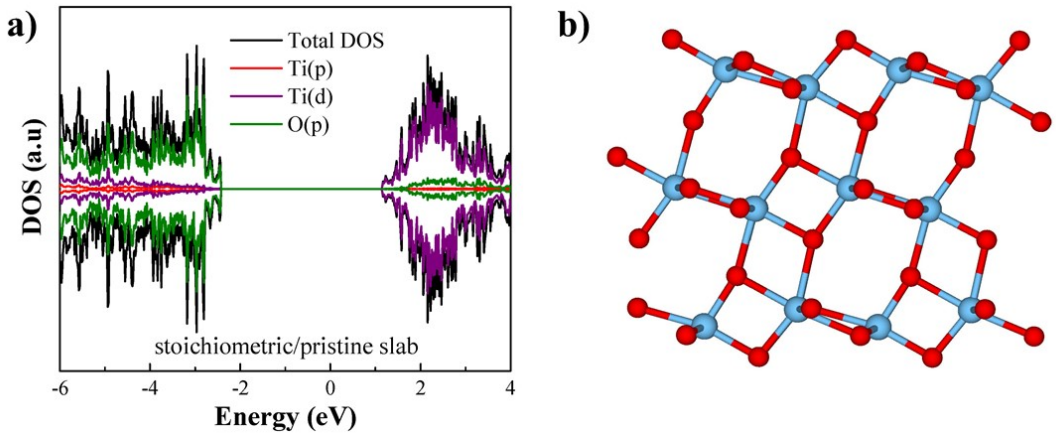

Figure S6-1. *(a) Density of states (DOS) and (b) side view of stoichiometric 1 x 3 anatase (101) slab. Red: titanium, cyan: oxygen atoms.*

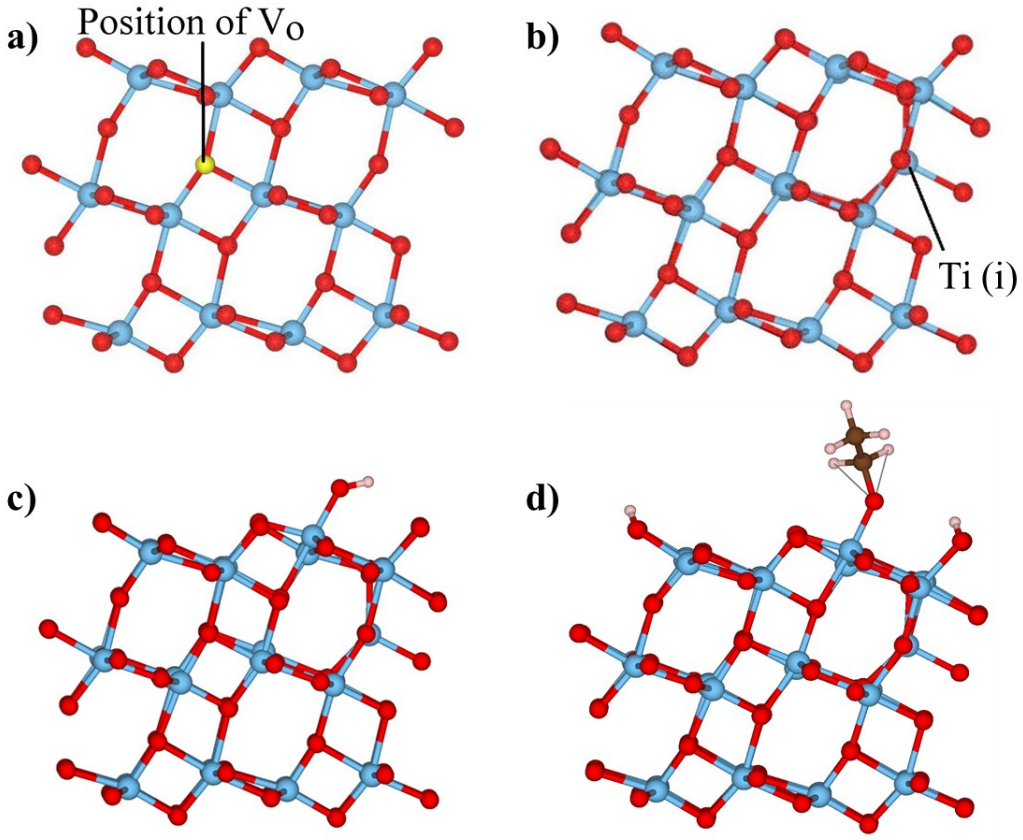

Figure S6-2. *Side view of (a) stoichiometric 1 x 3 anatase (101) slab, (b) defective slab with an oxygen vacancy (Vo-slab), (c) defective slab with a Ti interstitial (Ti(i)-slab); and, (c)*

adsorption of ethanol on defective slab with a Ti interstitial (Ti(i)-slab). Red: titanium, cyan: oxygen, brown: carbon, beige: hydrogen atoms; and, yellow: oxygen vacancy (Vo).

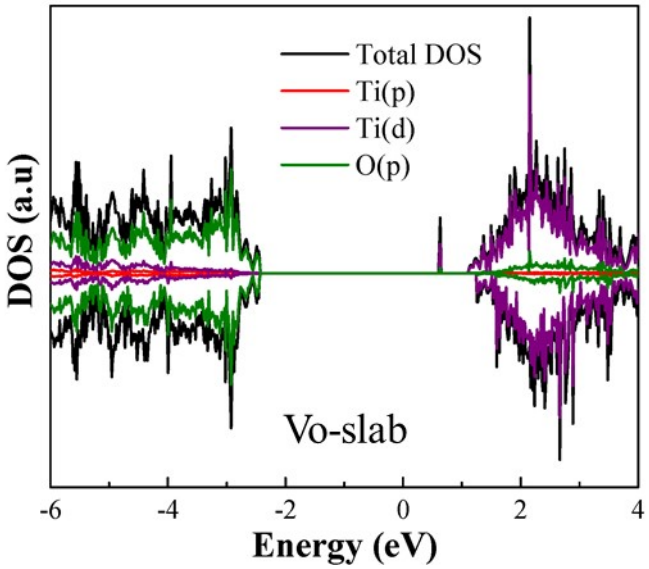

Figure S6-3. *(a) Density of states (DOS) plots of stoichiometric 1 x 3 anatase (101) slab with an oxygen vacancy (Vo).*

References

(1) Matěj, Z.; Kužel, R.; Nichtová, L. X-Ray Diffraction Analysis of Residual Stress in Thin Polycrystalline Anatase Films and Elastic Anisotropy of Anatase. *Metall and Mat Trans A* **2011**, *42* (11), 3323–3332. https://doi.org/10.1007/s11661-010-0468-z.

(2) Xu, S.; Tay, B. K.; Tan, H. S.; Zhong, L.; Tu, Y. Q.; Silva, S. R. P.; Milne, W. I. Properties of Carbon Ion Deposited Tetrahedral Amorphous Carbon Films as a Function of Ion Energy. *Journal of Applied Physics* **1996**, *79* (9), 7234–7240. https://doi.org/10.1063/1.361440.

(3) Sofi, A. H.; Shah, M. A.; Asokan, K. Structural, Optical and Electrical Properties of ITO Thin Films. *Journal of Elec Materi* **2018**, *47* (2), 1344–1352. https://doi.org/10.1007/s11664-017-5915-9.

(4) Davis, E. A.; Mott, N. F. Conduction in Non-Crystalline Systems V. Conductivity, Optical Absorption and Photoconductivity in Amorphous Semiconductors. *Philosophical Magazine* **1970**, *22* (179), 0903–0922. https://doi.org/10.1080/14786437008221061.

(5) Dow, J. D.; Redfield, D. Toward a Unified Theory of Urbach's Rule and Exponential Absorption Edges. *Phys. Rev. B* **1972**, *5* (2), 594–610. https://doi.org/10.1103/PhysRevB.5.594.